400 *Inorg. Chem.* **2011**, *50*, 400–402
DOI: 10.1021/ic101232u

Inorganic Chemistry
Communication

Guest-Specific Double- or Single-Step Adsorption in a Flexible Porous Framework Based on a Mixed-Ligand System

Prakash Kanoo, R. Sambhu, and Tapas Kumar Maji*

Molecular Materials Laboratory, Chemistry and Physics of Materials Unit, Jawaharlal Nehru Centre for Advanced Scientific Research, Jakkur, Bangalore 560 064, India

Received June 21, 2010

A 2D flexible metal−organic porous solid, $\{[Ni(1,3\text{-adc})(bpp)(H_2O)_2](H_2O)(EtOH)\}_n$ (**1**), has been synthesized using flexible organic linkers. The desolvated framework, $\{[Ni(1,3\text{-adc})(bpp)]\}_n$ (**1′**), undergoes structural contraction and exhibits double-step hysteretic adsorption for CO_2, H_2O, and MeOH and single-step gate-opening behavior with EtOH. These observations are correlated with the effect of the polarity and window dimension of the pore to the corresponding adsorbate molecules.

The flexible porous coordination polymers or metal−organic frameworks (MOFs) are so-called "third-generation coordination frameworks", as classified by Kitagawa et al., and are unique because of selective adsorption,[1] separation,[2] molecular recognition,[3] and specific sensing properties.[4] Such "soft porous materials" exhibit guest-induced structural contraction or expansion in the frameworks and offer unique adsorption phenomenon, like stepwise and gated adsorption with large hysteresis.[5] However, such guest adsorption and desorption processes are much more complicated than those observed in conventional rigid porous materials. Therefore, to design and fabricate such unique MOFs, we need to better understand their adsorption and desorption mechanisms, and analysis of these processes using the kinetics and thermodynamic approaches can provide detailed information.[6] MOFs with 2D networks show several guest-responsive dynamic phenomena related to interlayer separation, sliding, and rearrangement of the sheets,[7] and among them, only a few exhibit definite stepwise adsorption, which is related either to a "blocking effect" or to a "breathing effect".[8] The presence of weaker bonding interactions (e.g., hydrogen-bonding, $\pi-\pi$, and C−H$\cdots\pi$ interactions) in these structures allows them to orient in such a manner as to adapt according to the shape, size, and functionality of the guest molecules. Here in this Communication, we present the synthesis, structural characterization, and adsorbate-specific double-step (for CO_2, H_2O, and MeOH) or single-step (for EtOH) adsorption behavior in a 2D MOF material, $\{[Ni(1,3\text{-adc})(bpp)(H_2O)_2](H_2O)(EtOH)\}_n$ (**1**), constructed using flexible organic linkers [1,3-adc = 1,3-adamantanedicarboxylate;[9] bpp = 1,3-bis(4-pyridyl)propane]. The selectivity and unique adsorption behavior are correlated with the effect of the polarity and window dimension of the pore to the

*To whom correspondence should be addressed. E-mail: tmaji@jncasr.ac.in. Phone: +91 80 2208 2826. Fax: +91 80 2208 2766.

(1) (a) Kitagawa, S.; Kondo, M. *Bull. Chem. Soc. Jpn.* **1998**, *71*, 1739. (b) Ferey, G.; Serre, C. *Chem. Soc. Rev.* **2009**, *38*, 1380. (c) Ferey, G. *Chem. Soc. Rev.* **2008**, *37*, 191. (d) Maji, T. K.; Kitagawa, S. *Pure. Appl. Chem.* **2007**, *79*, 2155. (e) Kitagawa, S.; Uemura, K. *Chem. Soc. Rev.* **2005**, *34*, 109. (f) Bradshaw, D.; Claridge, J. B.; Cussen, E. J.; Prior, T. J.; Rosseinsky, M. J. *Acc. Chem. Res.* **2005**, *38*, 273.

(2) (a) Gurunatha, K. L.; Uemura, K.; Maji, T. K. *Inorg. Chem.* **2008**, *47*, 5678. (b) Horike, S.; Tanaka, D.; Nakagawa, K.; Kitagawa, S. *Chem. Commun.* **2007**, 3395. (c) Abrahams, B. F.; Moylan, M.; Orchard, S. D.; Robson, R. *Angew. Chem., Int. Ed.* **2003**, *42*, 1848. (d) Zhang, J.-P.; Chen, X.-M. *J. Am. Chem. Soc.* **2008**, *130*, 6010. (e) Maji, T. K.; Matsuda, R.; Kitagawa, S. *Nat. Mater.* **2007**, *6*, 142.

(3) (a) Pan, L.; Olson, D. H.; Ciemnolonski, L. R.; Heddy, R.; Li, J. *Angew. Chem., Int. Ed.* **2006**, *45*, 616. (b) Matsuda, R.; Kitaura, R.; Kitagawa, S.; Kubota, Y.; Kobayashi, T. C.; Horike, S.; Takata, M. *J. Am. Chem. Soc.* **2004**, *126*, 14063. (c) Maji, T. K.; Uemura, K.; Chang, H.-C.; Matsuda, R.; Kitagawa, S. *Angew. Chem., Int. Ed.* **2004**, *43*, 3269. (d) Serre, C.; Millange, F.; Thouvenot, C.; Nogues, M.; Marsolier, G.; Louer, D.; Férey, G. *J. Am. Chem. Soc.* **2002**, *124*, 13519. (e) Biradha, K.; Fujita, M. *Angew. Chem., Int. Ed.* **2002**, *41*, 3392.

(4) (a) Halder, G. J.; Kepert, C. J.; Moubaraki, B.; Murray, K. S.; Cashion, J. D. *Science* **2002**, *298*, 1762. (b) Maspoch, D.; Ruiz-Molina, D.; Wurst, K.; Domingo, N.; Cavallini, M.; Biscarini, F.; Tejada, J.; Rovira, C.; Veciana, J. *Nat. Mater.* **2003**, *2*, 190. (c) Wadas, T. J.; Wang, Q. M.; Kim, Y. J.; Flaschenrein, C.; Blanton, T. N.; Eisenberg, R. *J. Am. Chem. Soc.* **2004**, *126*, 16841.

(5) (a) Culp, J. T.; Smith, M. R.; Bittner, E.; Bockroth, B. *J. Am. Chem. Soc.* **2008**, *130*, 12427. (b) Choi, H. J.; Dincă, M.; Long, J. R. *J. Am. Chem. Soc.* **2008**, *130*, 7848. (c) Li, D.; Kaneko, K. *Chem. Phys. Lett.* **2001**, *335*, 50. (d) Gurunatha, K. L.; Maji, T. K. *Eur. J. Inorg. Chem.* **2009**, 1592. (e) Kitaura, R.; Fujimoto, K.; Noro, S.-i.; Kondo, M.; Kitagawa, S. *Angew. Chem., Int. Ed.* **2002**, *41*, 133. (f) Kanoo, P.; Gurunatha, K. L.; Maji, T. K. *J. Mater. Chem.* **2010**, *20*, 1322.

(6) (a) Tanaka, D.; Nakagawa, K.; Higuchi, M.; Horike, S.; Kubota, Y.; Kobayashi, T. C.; Takata, M.; Kitagawa, S. *Angew. Chem., Int. Ed.* **2008**, *47*, 3914. (b) Uemura, K.; Kitagawa, S.; Fukui, K.; Saito, K. *J. Am. Chem. Soc.* **2004**, *126*, 3817.

(7) (a) Biradha, K.; Hongo, Y.; Fujita, M. *Angew. Chem., Int. Ed.* **2002**, *41*, 3395. (b) Gurunatha, K. L.; Maji, T. K. *Inorg. Chem.* **2009**, *48*, 10886.

(8) (a) Uemura, K.; Yamasaki, Y.; Komagawa, Y.; Tanaka, K.; Kita, H. *Angew. Chem., Int. Ed.* **2007**, *46*, 6662. (b) Maji, T. K.; Mostafa, G.; Matsuda, R.; Kitagawa, S. *J. Am. Chem. Soc.* **2005**, *127*, 17152. (c) Kondo, A.; Hiroshi, N.; Carlucci, L.; Proserpio, D. M.; Ciani, G.; Kajiro, H.; Ohba, T.; Kanoh, H.; Kaneko, K. *J. Am. Chem. Soc.* **2007**, *129*, 12362. (d) Bourrelly, S.; Llewellyn, P. L.; Serre, C.; Millange, F.; Loiseau, T.; Férey, G. *J. Am. Chem. Soc.* **2005**, *127*, 13519.

(9) Jin, J.-C.; Zhang, Y.-N.; Wang, Y.-Y.; Liu, J.-Q.; Dong, Z.; Shi, Q.-Z. *Chem. Asian J.* **2010**, *5*, 1611.

Published on Web 12/16/2010

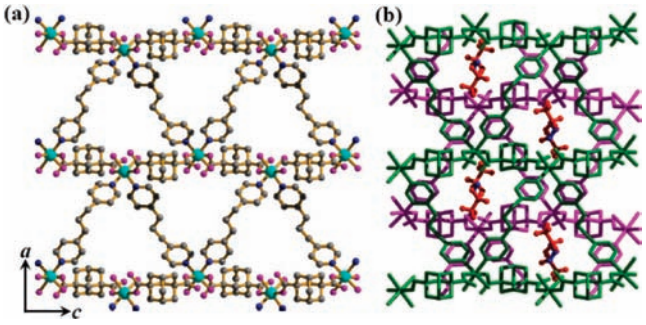

Figure 1. (a) 2D triangular sheet of **1** composed of 1D $[Ni(1,3\text{-adc})]_n$ chains connected by the bpp linkers. (b) 2D sheets stack along the *b* axis in an AB fashion, forming 1D channels occupied by H_2O (blue) and EtOH (red) molecules.

corresponding adsorbate molecules. Each step of the adsorption was monitored with a powder X-ray diffraction (PXRD) experiment, which suggested that at low $\sim P/P_0$ the pore is open to CO_2, H_2O, and MeOH but closed to EtOH molecules.

Compound **1** was synthesized by the reaction of $Ni(NO_3)_2 \cdot 6H_2O$ with 1,3-adc and bpp at room temperature in a H_2O/EtOH medium (Supporting Information, SI). X-ray structure determination[10] reveals that **1** crystallizes in orthorhombic space group $P2_12_12_1$ and the asymmetric unit is comprised of one Ni^{II} center, one 1,3-adc, one bpp, three H_2O molecules, and one EtOH molecule. Each octahedral Ni^{II} center is attached to two 1,3-adc (O1 and O4), two H_2O molecules (O5 and O6), and two bpp linkers (N1 and N2) (Figure S1 in the SI). The 1,3-adc ligands are in the trans position, whereas two H_2O molecules and two bpp nitrogen atoms are in the cis position around the Ni^{II} center. Ni1−O and Ni1−N distances are in the ranges of 2.041(3)−2.128(3) and 2.078(3)−2.091(3) Å, respectively. Ni^{II} and the 1,3-adc ligand form 1D chains along the *c* direction and are connected by the bpp linkers to generate a 2D triangular corrugated layer in the crystallographic *ac* plane (Figure 1a). Topological analysis with TOPOS[11] reveals a 4-connected uninodal **sql** net of triangular array restricted by the geometry of the 1,3-adc and bpp linkers (Figure S2 in the SI). The 2D corrugated layers are stacked in an AB fashion along the *b* direction and are interdigitated (Figures 1b and S3 in the SI). The interdigitation of the 2D layers supported by hydrogen-bonding and hydrophobic interactions results in the formation of a 3D supramolecular framework (Figure S3 in the SI). The 3D supramolecular framework provides 1D dumbbell-shaped channels of dimension 5.4 × 2.0 $Å^2$ along the *b* axis and is occupied by the guest H_2O and EtOH molecules (Figures 1b and S4 in the SI). The desolvated compound provides 22.12% void volume per unit cell volume, as calculated by *PLATON*.[12]

Thermogravimetric analysis (TGA) of **1** reveals a weight loss in the temperature range ~30−80 °C that corresponds to the loss of one EtOH and two coordinated H_2O molecules (weight loss: calcd 14.4%, obsd 13.8%; Figure S5 in the SI). The discrepancy in the TGA with regard to the unobserved loss of one guest H_2O molecule is probably because of its volatile nature. The desolvated compound **1′** is stable up to 380 °C. The PXRD pattern of **1′** shows sharp lines with the shifting of some Bragg peaks and also the appearance of some new peaks, suggesting structural transformation rather than collapse of the framework upon desolvation. After removal of the two coordinated H_2O molecules, the coordination environment of the Ni^{II} centers would be severely distorted. Consequently, there would be distortion also in the 2D network, which is responsible for the structural transformation. Indexing of the powder pattern of **1′** by the *TOPAS*[13] program suggests an orthorhombic crystal system similar to that of **1**, with a = 11.8123(91) Å, b = 14.4062(11) Å, c = 14.9962(13) Å, and V = 2551.90(36) $Å^3$ (see the SI). A decrease in the *a* and *b* parameters and a 9.5% reduction in the cell volume compared to **1** are indicative of structural contraction upon desolvation.

The excellent framework stability with coordinatively unsaturated Ni^{II} sites in **1′** provides an opportunity to establish permanent porosity and guest affinity depending upon the size and polarity of the different adsorbates. A N_2 (kinetic diameter = 3.6 Å)[14] adsorption isotherm for **1′** at 77 K shows no uptake by the framework (Figure S6 in the SI). However, CO_2 (3.3 Å) adsorption reveals a double-step profile at 195 K; a gradual uptake up to $P/P_0 \sim 0.13$ (21 mL g^{-1}) and then a steep rise in the second step lead to a final uptake volume of 100 mL g^{-1} (Figure S6 in the SI). A large hysteresis and sudden adsorption jump in the isotherm indicate structural transformation in the second step. The final uptake corresponds to 2.15 molecules of CO_2 per formula unit of **1′**, which relates to 20 wt % uptake by the framework. The selectivity of CO_2 over N_2 may be attributed to the smaller size and quadrupole moment of CO_2 (-1.4×10^{-39} C m^2) that interact with the unsaturated metal sites of the host network more effectively and lead to an opening of the channels at high P/P_0. The strong interaction of CO_2 with **1′** is also reflected in the high value of the isosteric heat of adsorption, q_{st}, ϕ (29 kJ mol^{-1}), as calculated by the Dubinin−Radushkevich equation.[15] Realizing a strong interaction between CO_2 and **1′**, the compound was tested for its adsorption properties toward different solvent molecules like H_2O (298 K), MeOH (293 K), and EtOH (298 K) having different polarities (Figures 2 and S8 and S9 in the SI). As anticipated, similar to the CO_2 isotherm, MeOH and H_2O adsorption measurements show a double-step profile; however, interestingly, the EtOH isotherm shows a single-step gated adsorption profile. Both H_2O (2.68 Å) and MeOH (4.0 Å) profiles reveal a gradual uptake at the low P/P_0 region, and the first-step adsorption corresponds to about 28.7 mL g^{-1} ($P/P_0 \sim 0.28$) and 33.5 mL g^{-1} ($P/P_0 \sim 0.18$) for H_2O and MeOH, respectively. In the second step, a steep uptake is observed in both cases with a final uptake volume of 131.5 mL g^{-1} (2.75 mol per Ni^{II}) and 205 mL g^{-1} (4.0 mol per Ni^{II}) for H_2O and MeOH, respectively. Notably, the first-step adsorption corresponds to the occlusion of 0.75 molecules of H_2O and MeOH per Ni^{II}. The desorption curve in the case of H_2O almost follows adsorption with a small hysteresis;

(10) Crystal data of **1**: formula $C_{27}H_{39}N_2NiO_8$, M_r = 578.29, orthorhombic, space group $P2_12_12_1$ (No. 19), a = 12.4421(3) Å, b = 15.0196(3) Å, c = 15.1013(3) Å, V = 2822.06(10) $Å^3$, Z = 4, $F(000)$ = 1228, total data = 24 620, unique data = 3321, R_{int} = 0.042, obsd data [$I > 2\sigma(I)$] = 3020, R = 0.0339, R_w = 0.0878, GOF = 0.73, Flack (x) = −0.005(19).

(11) (a) Blatov, V. A.; Carlucci, L.; Ciani, G.; Proserpio, D. M. *CrystEngComm* **2004**, *6*, 377. (b) Blatov, V. A.; Shevchenko, A. P.; Serezhkin, V. N. *J. Appl. Crystallogr.* **2000**, *33*, 1193.

(12) Spek, A. L. *J. Appl. Crystallogr.* **2003**, *36*, 7.

(13) *TOPAS*, version 4; Bruker AXS: Karlsruhe, Germany, 2008.

(14) Beck, D. W. *Zeolite Molecular Sieves*; John Wiley & Sons: New York, 1974.

(15) Dubinin, M. M. *Chem. Rev.* **1960**, *60*, 235.

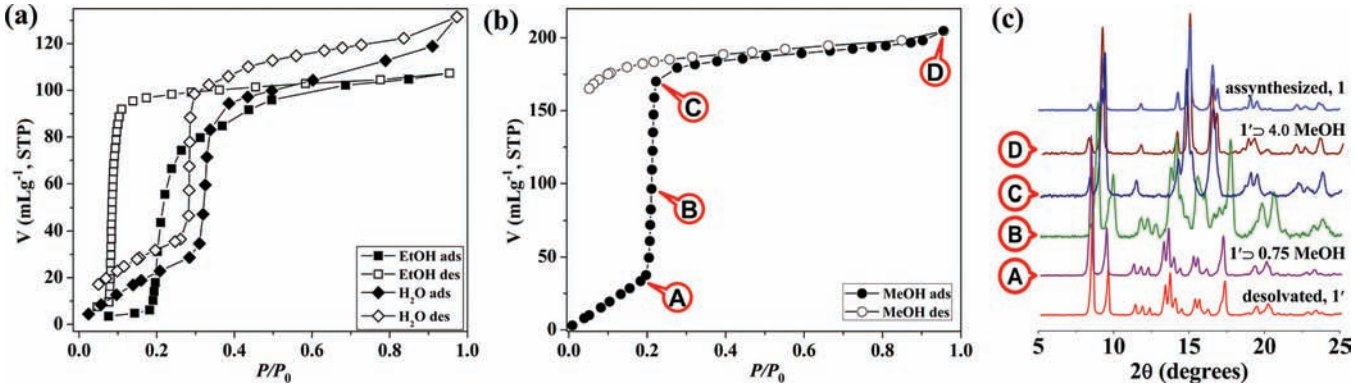

Figure 2. Vapor adsorption isotherms of **1′**: (a) H_2O and EtOH at 298 K; (b) MeOH at 293 K. P_0 is the saturated vapor pressure of the adsorbates at respective temperatures. (c) PXRD patterns of **1** and **1′** at different states of MeOH adsorption.

however, in the case of MeOH, desorption does not retrace the adsorption curve, and the compound retains ~165 mL g^{-1} of MeOH at $P/P_0 \sim 0.05$ at the end of adsorption. The incomplete desorption of MeOH suggests a strong interaction with the pore surface. Unlike H_2O and MeOH, EtOH (kinetic diameter, 4.3 Å) adsorption of **1′** reveals no uptake up to $P/P_0 \sim 0.18$; however, as the pressure increases further, a sudden adsorption jump is observed and the compound starts to adsorb rapidly and ends with a final uptake volume to ~107 mL g^{-1} at $P/P_0 \sim 0.97$.

To understand the adsorption process in detail, PXRD patterns of different vapor-adsorbed states of **1′** are recorded by interrupting the adsorption measurements at the desired points. Figure 2c shows PXRD patterns of **1**, **1′**, and different MeOH adsorbed states **A** (**1′**⊃0.75MeOH), **B**, **C**, and **D** (**1′**⊃4.0MeOH). The PXRD patterns of H_2O and EtOH adsorbed states of **1′** are given in Figure S8 in the SI. The PXRD patterns of the intermediate states **1′**⊃0.75MeOH and **1′**⊃0.75H_2O are similar to those of the desolvated state **1′**. Similarity in the indexed cell parameters of **1′**⊃0.75MeOH and **1′**⊃0.75H_2O with **1′** also supports this observation (see the SI). This suggests that the open channels in the shrunken state **1′** are accessible to small molecules like H_2O and MeOH but not to the larger EtOH molecule. However, after completion of the second step in the MeOH adsorption profile, the PXRD pattern of **1′**⊃4.0MeOH (point D) is almost similar to that of the as-synthesized compound **1**, suggesting structural transformation upon MeOH inclusion. The difference in the indexed cell parameters[13] of **1′**⊃4.0MeOH [a = 12.5063(20) Å, b = 14.8556(26) Å, c = 15.0106(24) Å, and V = 2788.78(80) Å^3] and **1′**⊃0.75MeOH also supports the structural transformation. Increases in the a and b parameters and unit cell volume compared to **1′** are indicative of a structural expansion upon MeOH inclusion. The PXRD patterns recorded at intermediate points in the second step during MeOH adsorption clearly indicate that structural transformation commences at or near point B and completes at point C. On the other hand, the PXRD pattern of **1′**⊃2.75H_2O is not similar to that of **1′** or **1** and the indexed cell parameter[16] of **1′**⊃2.75H_2O [a = 10.9444(81) Å, b = 13.1747(68) Å, c = 15.5292(78) Å, and V = 2239.15 Å^3 (see the SI)] but rather suggests structural contraction upon H_2O adsorption. This indicates that, although H_2O and MeOH adsorption profiles show double-step profiles, the mechanisms of adsorption are different. It is worth mentioning that the PXRD patterns of **1′**⊃2.75H_2O and **1′**⊃4.0MeOH are not similar, and this is further supported by different indexed cell parameters from the PXRD patterns. These results suggest that **1′** adsorbs H_2O molecules, maintaining a narrow pore; in contrast, MeOH molecules open the pore. Framework contraction upon H_2O adsorption is probably because of its strong coordinating ability toward the unsaturated Ni^{II} center and hydrogen-bonding interaction between the framework and adsorbed H_2O molecules in the pore. The higher uptake in the case of MeOH adsorption can be rationalized by taking into consideration both hydrophobic and hydrophilic interaction through $-CH_3$ and $-OH$ groups, respectively, with the framework. Because larger EtOH molecules hardly penetrate into the narrow pore, an initial uptake is not observed in the isotherm of **1′**, only exhibiting single-step gate-opening behavior.

In summary, a new 2D coordination network of Ni^{II} has been synthesized that was found to be very flexible and exhibit double- or single-step adsorption characteristics for small molecules. This type of guest-specific response is very unique and would provide a better understanding for the design and synthesis of new materials that would show guest-dependent dynamic behavior and may find application as actuators, in molecular recognition, and in specific sensing.

Acknowledgment. T.K.M. is grateful to DST for financial support (fast track proposal). P.K. acknowledges CSIR, India, for SRF. R.S. is thankful to JNCASR for the POCE program.

Supporting Information Available: Details of the experimental procedure, Figures S1−S13, Tables 1 and 2, and X-ray crystallographic file in CIF format for **1**. This material is available free of charge via the Internet at http://pubs.acs.org.

(16) Boultif, A.; Louer, D. *J. Appl. Crystallogr.* **2004**, *37*, 724.